Harnessing the Anti-Cancer Natural Product Nimbolide for Targeted Protein Degradation

Jessica N. Spradlin[1,2], Xirui Hu[1,2], Carl C. Ward[2,3], Scott M. Brittain[2,4], Lisha Ou[1,2], Dirksen E. Bussiere[2,5], Jason R. Thomas[2,4,6], John A. Tallarico[2,4], Jeffrey M. McKenna[2,4], Markus Schirle[2,4], Thomas J. Maimone[1,2,*], and Daniel K. Nomura[1,2,3,7,*]

[1] Department of Chemistry, University of California, Berkeley, Berkeley, CA 94720

[2] Novartis-Berkeley Center for Proteomics and Chemistry Technologies

[3] Department of Molecular and Cell Biology, University of California, Berkeley, Berkeley, CA 94720

[4] Novartis Institutes for BioMedical Research, Cambridge, MA 02139

[5] Novartis Institutes for BioMedical Research, Emeryville, CA 94608

[6] Current address: Vertex Pharmaceuticals, Boston, MA 02210

[7] Department of Nutritional Sciences and Toxicology, University of California, Berkeley, Berkeley, CA 94720

*correspondence to maimone@berkeley.edu and dnomura@berkeley.edu

Keywords: nimbolide, chemoproteomics, RNF114, ZNF313, activity-based protein profiling, ABPP, degraders, targeted protein degradation

Abstract

Nimbolide, a terpenoid natural product derived from the Neem tree, impairs cancer pathogenicity across many types of human cancers; however, the direct targets and mechanisms by which nimbolide exerts its effects are poorly understood. Here, we used activity-based protein profiling (ABPP) chemoproteomic platforms to discover that nimbolide reacts with a novel functional cysteine crucial for substrate recognition in the E3 ubiquitin ligase RNF114. Nimbolide impairs breast cancer cell proliferation by disrupting RNF114 substrate recognition, leading to inhibition of ubiquitination and degradation of the tumor-suppressor p21, resulting in its rapid stabilization. We further demonstrate that nimbolide can be harnessed to recruit RNF114 as an E3 ligase in targeted protein degradation applications and show that synthetically simpler scaffolds are also capable of accessing this unique reactive site. Our study highlights the utility of ABPP platforms in uncovering unique druggable modalities accessed by natural products for cancer therapy and drug discovery applications.

Introduction

Natural products from organisms such as plants and microbes are a rich source of therapeutic lead compounds [1–5]. The characterization of their biological activities has resulted in myriad medications for disparate pathologies such as cancer, bacterial and fungal infections, inflammation, and diabetes [1–5]. Among natural products there exists a subset of covalently acting molecules that bear electrophilic moieties capable of undergoing essentially irreversible reactions with nucleophilic amino acid hotspots within proteins to exert their therapeutic activity. Examples of these natural products include penicillin, which irreversibly inhibits serine transpeptidases inducing anti-bacterial activity, or wortmannin, which covalently modifies a functional lysine on PI3-kinase to inhibit its activity [5–7]. Discovering druggable hotspots targeted by anti-cancer and covalently-acting natural products can not only yield new cancer drugs and therapeutic targets but can also reveal unique insights into modalities accessed by natural products in protein targets that are often considered undruggable or difficult to tackle with standard drug discovery efforts. One example of a druggable modality that would be difficult to predict *a priori* is FK506 or Tacrolimus that inhibits peptidylprolyl isomerase activity by binding to FKBP12 thus creating a FKBP12-FK506 complex that modulates T cell signaling via inhibition of calcineurin [8]. Gaining insights into nature's strategies for engaging protein targets can thus provide access to new perspectives on what may be considered druggable.

In this study, we investigated the mechanism of action of the natural product nimbolide, a limonoid natural product derived from the Neem tree (*Azadirachta indica*) **(Figure 1A)** [9]. Nimbolide has been shown to exert multiple therapeutic effects and possesses a cyclic enone capable of reacting with cysteines [10–12]. In the context of cancer, nimbolide has been shown to inhibit tumorigenesis and metastasis without causing any toxicity or unwanted side effects across a wide range of cancers [10,11,13–17]. While previous studies suggest that nimbolide impairs cancer pathogenicity through modulating signaling pathways and transcription factors linked to survival, growth, invasion, angiogenesis, inflammation, and oxidative stress the direct targets of nimbolide still remain poorly characterized [10,15,18–22].

Identifying direct protein targets of complex natural products remains challenging and often requires synthesizing analogs of these compounds bearing photoaffinity and enrichment handles, a task which is synthetically challenging and has the potential to alter the activity of the molecule [23–25]. Even with the generation of such probes, identifying the specific amino acid site targeted by natural products is challenging.

In this study, we utilized activity-based protein profiling (ABPP) chemoproteomic approaches to map the proteome-wide targets of nimbolide in breast cancer cell proteomes. Using ABPP platforms, we reveal that one of the primary targets of nimbolide in breast cancer cells is cysteine-8 (C8) of the E3 ubiquitin ligase RNF114. Covalent modification of RNF114 by nimbolide leads to impaired ubiquitination and degradation of its substrate—the tumor suppressor p21—leading to its rapid stabilization. Intriguingly, we show that this apparent inhibition of RNF114 activity is through impaired substrate recognition giving rise to the possibility that nimbolide could be used as an E3 ligase recruitment module for targeted protein degradation. Strategies for chemically induced degradation of targets of interest in cells is rapidly gaining interest in drug discovery, including the development of bifunctional molecules referred to as "proteolysis-targeting chimeras" (PROTACs) or "heterobifunctional degraders" that consist of a protein-targeting ligand linked to an E3 ligase recruiter to bring an E3 ligase to a protein of interest to ubiquitinate and mark the target for degradation in a proteasome-dependent manner [26–34]. We demonstrate that nimbolide can be used to recruit RNF114 to other protein substrates for targeted protein degradation applications. Using chemoproteomics-enabled covalent ligand screening platforms, we also identify more synthetically tractable compounds that can similarly react with C8 of RNF114 and phenocopy nimbolide action.

Results

Effects of nimbolide on breast cancer cell survival and proliferation

Though nimbolide has been shown to impair cancer pathogenicity across many different types of human cancers, we chose to focus on elucidating the role of nimbolide in triple-negative breast cancers (TNBC). TNBCs are devoid of estrogen, progesterone, and HER2 receptors and are amongst the most aggressive cancers with the worst clinical prognosis [35,36]. Very few targeted therapies currently exist for TNBC patients. Uncovering new therapeutic modalities in TNBCs would thus potentially contribute significantly to reducing breast cancer-associated mortalities. Consistent with previous reports showing anti-cancer activity in breast cancer cells, nimbolide impaired cell proliferation or serum-free cell survival in 231MFP and HCC38 TNBC cells **(Figure 1B)** [14,15,17].

Using ABPP platforms to map druggable hotspots targeted by nimbolide in breast cancer cells

To interrogate the mechanisms by which nimbolide impairs breast cancer pathogenicity, we applied a chemoproteomic platform termed isotopic tandem orthogonal proteolysis-enabled activity-based protein profiling (isoTOP-ABPP) to determine the specific protein targets of nimbolide. Pioneered by Cravatt and Weerapana, isoTOP-ABPP uses reactivity-based chemical probes to map reactive, functional, and druggable hotspots directly in complex proteomes [37–40]. When used in a competitive manner, covalently-acting small-molecules can be competed against reactivity-based probe binding to facilitate target identification [40–47] **(Figure 2A)**. In this study, we treated breast cancer cells *in situ* with vehicle or nimbolide followed by competitive labeling of proteomes with a cysteine-reactive alkyne-functionalized iodoacetamide probe (IA-alkyne), after which isotopically light or heavy cleavable enrichment handles were appended to probe-labeled proteins for isoTOP-ABPP analysis. Probe-modified tryptic peptides were analyzed by liquid chromatography-mass spectrometry (LC-MS/MS) and light to heavy tryptic probe-modified peptide ratios, representing control versus treated IA-alkyne labeled sites, were quantified. IsoTOP-ABPP analysis of ligandable hotspots targeted by *in situ* nimbolide treatment in 231MFP TNBC cells showed two targets showing isotopic ratios >4— namely RNF114 and HPCAL1 **(Figure 2B; Table S1)**. Importantly, RNF114 knockdown using RNA interference closely resembled the anti-proliferative effects of nimbolide in 231MFP cells, indicating that RNF114 is likely to constitute the primary efficacy target of nimbolide **(Figure 2C)**. Further supporting this hypothesis, RNF114 was the target responsible for nimbolide action, RNF114 knockdown led to significantly heightened sensitivity to nimbolide-mediated anti-proliferative effects **(Figure 2D)**. We thus chose to focus further characterization efforts upon RNF114.

Biochemical characterization of nimbolide interactions with RNF114

RNF114 is an E3 ubiquitin ligase of the RING family [48,49]. The site on RNF114 identified by isoTOP-ABPP as the target of nimbolide, C8, falls within the N-terminal region of the protein, predicted to be intrinsically disordered, and resides outside of the two annotated zinc finger domains **(Figure 3A)**. Intrigued by the apparent selective targeting of an intrinsically disordered region of a protein by a natural product, we sought to investigate the interaction between nimbolide and RNF114.

Because isoTOP-ABPP is a competitive assay between the covalently-acting molecule and a broader reactive probe, it is an indirect read-out of potential nimbolide-targeting hotspots. To confirm that nimbolide

directly targeted RNF114, we synthesized the alkyne-functionalized probe shown in three steps from nimbolide (**Figure 3B**). Selective bromination at C2 of the furan moiety and subsequent Suzuki coupling with 4-Formylphenylboronic acid afforded the aryl-aldehyde **2**, which was converted to its corresponding carboxylic acid (**3**) via Pinnick oxidation. Finally, coupling of **3** and propargyl amine (HATU, DIPEA) afforded the target probe. We confirmed that this nimbolide probe reacts with pure human RNF114 protein. This labeling event was also competed by nimbolide and abrogated in the C8A RNF114 mutant **(Figure 3C)**. Furthermore, a direct mass adduct of nimbolide on C8 of RNF114 was observed by LC-MS/MS after incubation of pure protein with the natural product **(Figure 3D)**. Taken together, these findings provide convincing evidence that nimbolide modifies an intrinsically disordered region of RNF114 at C8 through a covalent bond formation.

Effects of nimbolide on RNF114 activity and substrate binding *in vitro* and *in situ*

RNF114 has been previously shown to ubiquitinate and degrade the tumor suppressor p21, among other substrates [48,50,51]. In an *in vitro* reconstituted system, nimbolide inhibited both RNF114 autoubiquitination and p21 ubiquitination activity **(Figure 4A)**. The RNF114 C8A mutation did not affect basal RNF114 autoubiquitination activity, but attenuated the inhibition observed with nimbolide treatment **(Figure 4B)**. Previous characterization of RNF114 suggested that the N-terminus may be involved in substrate recognition [48]. Consistent with this premise, we found that the amount of p21 co-immunoprecipitated with RNF114 was reduced by nimbolide, suggesting that the apparent inhibition of RNF114 may be due to impaired substrate recognition, rather than inhibition of its catalytic activity **(Figure 4C)**. We further demonstrated that nimbolide treatment in 231MFP cells stabilized p21 protein expression within 1 hour, with no significant changes to p53 levels **(Figure 4D, Figure S1)**. Collectively, this data suggests that nimbolide reacts with an intrinsically disordered C8 of RNF114 to disrupt RNF114-p21 substrate recognition, leading to inhibition of p21 ubiquitination, rapid p21 stabilization, and impaired cell proliferation in breast cancer cells.

Using nimbolide as an RNF114-recruiter for targeted protein degradation

Since nimbolide targets a potential substrate recognition site, we conjectured that nimbolide could be used to recruit RNF114 to other protein substrates for proteasomal degradation through the development of bifunctional degraders using nimbolide as an RNF114 recruiter. To demonstrate feasibility, two degraders

formed by linking nimbolide to the Bromodomain and extra-terminal (BET) family inhibitor JQ1 were synthesized **(Figure 5A; Figure S2A)**. Prior studies have demonstrated efficient proteasome-dependent degradation of BET family members and in particular BRD 4 with JQ1-based degraders linked to either a cereblon-recruiter thalidomide or a VHL recruiter [27,30,34]. Previously prepared acid **3** was coupled to JQ1-functionalized amines containing both longer (PEG-based) and shorter (alkyl-based) spacer units, arriving at degraders **XH1** and **XH2 (Figure 5A; Figure S2A)**. While **XH1** did not show appreciable BRD4 degradation, **XH2** treatment in 231MFP cells led to BRD4 degradation after a 12 h, but not 8 h treatment **(Figure 5B; Figure S2B, 8 h data not shown)**. Comparing the dose-response of BRD4 degradation between **XH2** to a previously reported JQ1-based degrader MZ1 that utilizes a VHL recruiter, we showed that **XH2** showed better BRD4 degradation compared to MZ1 at 10 nM, but MZ1 showed better BRD4 degradation at 1 and 0.1 μM compared to **XH2 (Figure 5B)**. Interestingly, **XH2** showed less degradation at 1 μM compared to 0.1 and 0.01 μM and MZ1 showed less degradation at 20 μM compared to 10, 1, and 0.1 μM, which we attribute to the "hook effect" previously reported with degraders including MZ1 [26,27]. To confirm proteasome-dependence of BRD4 degradation, we showed that the **XH2**-mediated degradation of BRD4 was attenuated by pre-treatment of cells with the proteasome inhibitor bortezomib (BTZ) **(Figure 5C)**. **XH2**-mediated BRD4 degradation was also prevented by pre-treatment with an E1 ubiquitin-activating enzyme inhibitor (TAK-243) or pre-competing with the BRD4 inhibitor JQ1 **(Figure 5D, Figure S2C)**. However, treatment with a translation inhibitor (emetine) had no effect of the observed degradation of BRD4 **(Figure S2D)**. To further demonstrate that the degradation of BRD4 by **XH2** was through the specific recruitment of RNF114, we showed that degradation of BRD4 by **XH2**, but not MZ1, was not observed in RNF114 knockout (KO) HAP1 cells compared to wild-type (WT) HAP1 cell counterparts **(Figure 5E)**. The selectivity of **XH2**-mediated degradation of proteins was demonstrated using tandem mass tagging (TMT)-based quantitative proteomic profiling experiment to assess changes in protein expression. We showed that **XH2** selectively degrades BRD4 in 231MFP breast cancer cells while sparing the other identified BET family members BRD 2 and 3 **(Figure 5F)**. Of note, we also observed several proteins that showed increased levels upon **XH2** treatment--including p21 (CDKN1A) which we had observed previously with nimbolide treatment alone. These upregulated proteins may be potential substrates of RNF114 with stabilization stemming from the nimbolide portion of XH2 or downstream transcriptional effects stemming from JQ1-mediated BRD4 inhibition and degradation. If these proteins were RNF114 substrates, we would expect

these proteins to be elevated with nimbolide treatment alone. We thus performed a TMT-based quantitative proteomic experiment on 231MFP cells treated with nimbolide. Consistent with our premise, protein levels of several of the targets upregulated with XH2 treatment were also increased with nimbolide treatment alone, including CDKN1C, CDKN1A, PEG10, and CTGF. Beyond CDKN1A (p21) and CDKN1C (p57) which have previously been reported as potential RNF114 substrates [48], PEG10 and CTGF may represent additional novel substrates of RNF114 **(Figure 5G)**. Our results strongly suggest that nimbolide reactivity with C8 of RNF114 can be exploited to recruit this E3 ligase to other protein substrates, such as BRD4, to ubiquitinate and selectively degrade them.

Chemoproteomics-enabled covalent ligand screening to identifying covalent ligands against RNF114

With the insight gained that C8 of RNF114 has potential to be exploited for cancer therapy and targeted protein degradation applications, we searched for more synthetically tractable covalent ligands that similarly target RNF114. To achieve this goal, we screened a library of cysteine-reactive covalent ligands against RNF114 using a moderate-throughput gel-based ABPP approach, in which covalent ligands are competed against IA-alkyne labeling of RNF114, followed by appending a rhodamine-azide and analysis by SDS/PAGE and in-gel fluorescence. Initial studies competing nimbolide against IA-alkyne labeling of RNF114 did not show full inhibition of labeling, likely due to alkylation of multiple cysteines by IA-alkyne beyond C8. Thus, we synthesized a more tailored alkyne-functionalized cyclic enone probe JNS27, which showed selective labeling of C8 on RNF114 as evidenced by lack of labeling of C8A RNF114 mutant protein and the observed full competition with nimbolide **(Figure 6A)**. Of the approximately 200 cysteine-reactive covalent ligands screened against RNF114, the acrylamide **EN62** emerged as a promising hit **(Figure 6B; Figure S3)**. **EN62** inhibited RNF114 autoubiquitination activity in a C8-dependent manner and also exhibited proteome-wide selectivity in 231MFP breast cancer cell proteomes **(Figure 6C-6D)**. **EN62** also impaired 231MFP breast cancer cell survival and attenuated *in vivo* 231MFP tumor xenograft growth in immune-deficient mice **(Figures 6E-6F)**. While **EN62** requires further improvements to potency, this covalent ligand represents a more synthetically tractable starting point for future cancer therapy and protein degradation applications.

Discussion

Collectively, we show compelling evidence that nimbolide impairs breast cancer pathogenicity in-part through targeting a substrate recognition domain at C8 within RNF114 to inhibit p21 ubiquitination and degradation, leading to its stabilization. We demonstrate that nimbolide targeting of C8 on RNF114 can be used to recruit RNF114 for targeted protein degradation applications and degradation of BRD4 with a nimbolide-JQ1 degrader **XH2** is possible. Additionally, using chemoproteomics-enabled covalent ligand screening approaches, we show proof-of-concept that more synthetically tractable covalent ligands, such as **EN62**, can be rapidly identified to target druggable sites employed by complex natural products, such as C8 of RNF114.

We report here that nimbolide disrupts RNF114 interactions with one of its endogenous substrate p21 and we also show that p21 levels are rapidly stabilized in breast cancer cells in a p53-independent manner. Several other E3 ligases have also been reported to degrade p21, including SCF^{Skp2}, $CRL4^{Cdt2}$, and CHIP under varying conditions during cell cycle or exogenous stress [52–54]. Previous studies have shown that RNF114 expression is elevated at late G1 phase to regulate p21 levels and is crucial for G1-to-S phase transition [48]. Other RNF114 substrates that have been reported include TAB1 involved in maternal-to-zygotic transition and A20 involved in NF-κB activity and T cell activation [55,56]. In cancer contexts or other cell and tissue types, nimbolide may thus have additional activities through regulating the levels of other RNF114 protein substrates. Intriguingly, we show several proteins heightened in expression with **XH2** treatment, including previously reported RNF114 substrates p21 (CDKN1A) and p57 (CDKN1C), as well as several other proteins **(Figure 5F)**. These proteins may represent additional substrates of RNF114. Consistent with this premise, we also observe p21, p57, and CTGF and PEG10 levels heightened with nimbolide treatment alone **(Figure 5G).** Further studies are required to establish these additional proteins as direct substrates of RNF114. Furthermore, while we show that RNF114 is one of the primary functional targets of nimbolide, there may be additional protein targets that may not have been readily identified using this method due to reversibility or IA-probe limitations. Nonetheless, we demonstrate that RNF114 is an important and functional target of nimbolide in breast cancer cell proliferation, since knockdown of RNF114 hypersensitized the cells to nimbolide.

Our results also demonstrate that nimbolide functionally targets an intrinsically disordered region within RNF114. Solving the structure of RNF114 covalently modified with nimbolide has thus far proven challenging, but future studies investigating whether nimbolide induces order in the N-terminus would provide insights into

the ligandability of intrinsically disordered and undruggable protein targets and strategies for potentially targeting other E3 ligases.

Targeted protein degradation has emerged as a formidable and effective drug discovery paradigm for targeting proteins for elimination through the proteasome [26,28]. One of the challenges, however, is that there are only a small number of E3 ligase recruiters that have been developed among the approximately 600 E3 ligases in the human genome [57]. These E3 ligase recruiters include the thalidomide-type immunomodulatory drugs (IMiD) that recruit cereblon, ligands that recruit VHL, nutlins that recruit MDM2, and ligands that recruit cIAP [26,28]. Here, we report that nimbolide can be used as a novel RNF114 recruiter for targeted protein degradation applications. It should be possible to optimize the performance of this degrader class *via* further linker modifications, an area of the molecule already determined to be important. It may also be possible to utilize more synthetically tractable covalent ligands capable of targeting C8 of RNF114, such as EN62, as RNF114 recruiters. Since nimbolide targets a substrate recognition domain within RNF114, it will also be of future interest to determine whether nimbolide may act as a molecular glue to recruit and degrade neo-substrates, as has been reported for the IMiDs [58–60].

Interestingly, we did not observe degradation of BRD2 and 3 under conditions that led to significant reduction of BRD4 levels despite the high homology in their respective BET bromodomains. Various levels of selectivity within the BET family members and the structural basis thereof have been reported for JQ1-based degraders with Cereblon and VHL-recruiting modules [27,30,61,62]. While a more detailed investigation of the selectivity of XH2 and its structural basis is outside the scope of this study, it serves as another example how availability of additional E3-moieties for a given substrate recognition modules can aid in tuning efficacy and selectivity of degraders targeting a given protein of interest.

Overall, our study further demonstrates the utility of using ABPP-based chemoproteomic platforms to identify unique druggable modalities exploited by natural products. Intriguingly, we show that a natural product can functionally access an E3 ligase protein-protein interaction site for potential cancer therapy and targeted protein degradation applications and remarkably does so in an intrinsically disordered region of the protein. Our study also showcases how covalent ligand screening approaches can be utilized to identify more synthetically tractable small-molecules that act similarly to more complex natural products and that covalent ligands may be able to access other E3 ligases to expand the scope of E3 ligase recruiters.

Methods

Cell Culture

The 231MFP cells were obtained from Prof. Benjamin Cravatt and were generated from explanted tumor xenografts of MDA-MB-231 cells as previously described [63]. HCC38 and HEK293T cells were obtained from the American Type Culture Collection. HEK293T cells were cultured in DMEM containing 10% (v/v) fetal bovine serum (FBS) and maintained at 37°C with 5% CO_2. 231MFP were cultured in L15 medium containing 10% FBS and maintained at 37°C with 0% CO_2. HCC38 cells were cultured in RPMI medium containing 10% FBS and maintained at 37°C with 5% CO_2. HAP1 RNF114 wild-type and knockout cell lines were purchased from Horizon Discovery. The RNF114 knockout cell line was generated by CRISPR/Cas9 to contain a frameshift mutation in a coding exon of RNF114. HAP1 cells were grown in Iscove's Modified Dulbecco's Medium (IMDM) in the presence of 10 % FBS and penicillin/streptomycin.

Survival and Proliferation Assays

Cell survival and proliferation assays were performed as previously described using Hoechst 33342 dye (Invitrogen) according to manufacturer's protocol and as previously described [64]. 231MFP cells were seeded into 96-well plates (40,000 for survival and 20,000 for proliferation) in a volume of 150 µl and allowed to adhere overnight. Cells were treated with an additional 50 µL of media containing 1:250 dilution of 1000 x compound stock in DMSO. After the appropriate incubation period, media was removed from each well and 100 µl of staining solution containing 10% formalin and Hoechst 33342 dye was added to each well and incubated for 15 min in the dark at room temperature. After incubation, staining solution was removed, and wells were washed with PBS before imaging. Studies with HCC38 cells were also performed as above but were seeded with 20,000 cells for survival and 10,000 cells for proliferation.

IsoTOP-ABPP chemoproteomic studies

IsoTOP-ABPP studies were done as previously reported [37,40,44,65]. Cells were lysed by probe sonication in PBS and protein concentrations were measured by BCA assay [66]. For *in situ* experiments, cells were treated for 90 min with either DMSO vehicle or covalently-acting small molecule (from 1000X DMSO stock) before cell

collection and lysis. For *in vitro* experiments, proteome samples diluted in PBS (4 mg of proteome per biological replicate) were treated with a DMSO vehicle or covalently-acting small-molecule for 30 min at room temperature. Proteomes were subsequently labeled with IA-alkyne labeling (100 μM) for 1 h at room temperature. CuAAC was used by sequential addition of tris(2-carboxyethyl)phosphine (1 mM, Sigma), tris[(1-benzyl-1H-1,2,3-triazol-4-yl)methyl]amine (34 μM, Sigma), copper (II) sulfate (1 mM, Sigma), and biotin-linker-azide—the linker functionalized with a TEV protease recognition sequence as well as an isotopically light or heavy valine for treatment of control or treated proteome, respectively. After CuAAC, proteomes were precipitated by centrifugation at 6500 x g, washed in ice-cold methanol, combined in a 1:1 control/treated ratio, washed again, then denatured and resolubilized by heating in 1.2 % SDS/PBS to 80°C for 5 minutes. Insoluble components were precipitated by centrifugation at 6500 x g and soluble proteome was diluted in 5 ml 0.2% SDS/PBS. Labeled proteins were bound to avidin-agarose beads (170 μl resuspended beads/sample, Thermo Pierce) while rotating overnight at 4°C. Bead-linked proteins were enriched by washing three times each in PBS and water, then resuspended in 6 M urea/PBS (Sigma) and reduced in TCEP (1 mM, Sigma), alkylated with iodoacetamide (IA) (18 mM, Sigma), then washed and resuspended in 2 M urea and trypsinized overnight with 0.5 μg/μl sequencing grade trypsin (Promega). Tryptic peptides were eluted off. Beads were washed three times each in PBS and water, washed in TEV buffer solution (water, TEV buffer, 100 μM dithiothreitol) and resuspended in buffer with Ac-TEV protease and incubated overnight. Peptides were diluted in water and acidified with formic acid (1.2 M, Spectrum) and prepared for analysis.

Mass Spectrometry Analysis

Peptides from all chemoproteomic experiments were pressure-loaded onto a 250 μm inner diameter fused silica capillary tubing packed with 4 cm of Aqua C18 reverse-phase resin (Phenomenex # 04A-4299) which was previously equilibrated on an Agilent 600 series HPLC using gradient from 100% buffer A to 100% buffer B over 10 min, followed by a 5 min wash with 100% buffer B and a 5 min wash with 100% buffer A. The samples were then attached using a MicroTee PEEK 360 μm fitting (Thermo Fisher Scientific #p-888) to a 13 cm laser pulled column packed with 10 cm Aqua C18 reverse-phase resin and 3 cm of strong-cation exchange resin for isoTOP-ABPP studies. Samples were analyzed using an Q Exactive Plus mass spectrometer (Thermo Fisher Scientific) using a 5-step Multidimensional Protein Identification Technology (MudPIT) program, using 0

%, 25 %, 50 %, 80 %, and 100 % salt bumps of 500 mM aqueous ammonium acetate and using a gradient of 5-55 % buffer B in buffer A (buffer A: 95:5 water:acetonitrile, 0.1 % formic acid; buffer B 80:20 acetonitrile:water, 0.1 % formic acid). Data was collected in data-dependent acquisition mode with dynamic exclusion enabled (60 s). One full MS (MS1) scan (400-1800 m/z) was followed by 15 MS2 scans (ITMS) of the nth most abundant ions. Heated capillary temperature was set to 200 °C and the nanospray voltage was set to 2.75 kV.

Data was extracted in the form of MS1 and MS2 files using Raw Extractor 1.9.9.2 (Scripps Research Institute) and searched against the Uniprot human database using ProLuCID search methodology in IP2 v.3 (Integrated Proteomics Applications, Inc) [67]. Cysteine residues were searched with a static modification for carboxyaminomethylation (+57.02146) and up to two differential modifications for methionine oxidation and either the light or heavy TEV tags (+464.28596 or +470.29977, respectively). Peptides were required to have at least one tryptic end and to contain the TEV modification. ProLUCID data was filtered through DTASelect to achieve a peptide false-positive rate below 5%. Only those probe-modified peptides that were evident across all two out of three biological replicates were interpreted for their isotopic light to heavy ratios. Those probe-modified peptides that showed ratios >3 were further analyzed as potential targets of the covalently-acting small-molecule. For modified peptides with ratios >3, we filtered these hits for peptides were present in all three biological replicates. For those probe-modified peptide ratios >3, only those peptides with 3 ratios >3 were interpreted, and otherwise replaced with the lowest ratio. For those probe-modified peptide ratios >4, only those peptides with 3 ratios >4 were interpreted, and otherwise replaced with the lowest ratio. MS1 peak shapes of any resulting probe-modified peptides with ratios >3 were then manually confirmed to be of good quality for interpreted peptides across all biological replicates.

Constructing knockdown lines

We used short-hairpin oligonucleotides to knock down the expression of RNF114 in 231MFP cells using previously described methods [68]. For generation of stable shRNA lines, lentiviral plasmids in the pLKO.1 backbone containing shRNA (Sigma) against human RNF114 were transfected into HEK293T cells using Lipofectamine (Invitrogen). Lentivirus was collected from filtered cultured medium and used to infect the target

cancer cell line with Polybrene. Target cells were selected over 3 days with 1 µg/ml puromycin. The short-hairpin sequence used for generation of the RNF114 knockdown lines was: CCGGCCATGGCTGCCGTAAGAATTTCTCGAGAAATTCTTACGGCAGCCATGGTTTTTG (Sigma RNF114 MISSION shRNA Bacterial Glycerol Stock, TRCN0000314877).

The control shRNA was targeted against GFP with the target sequence GCAAGCTGACCCTGAAGTTCAT. Knockdown was confirmed by qPCR.

Gene Expression by qPCR

Gene expression was confirmed by qPCR using the manufacturer's protocol for Fisher Maxima SYBR Green. Primer sequences for Fisher Maxima SYBR Green were derived from Primer Bank. Sequences of primers are as follows:

RNF114 Forward: AAT GTT CCA AAC CG

RNF114 Reverse: TTG CAG TGT TCC AC

Cyclophilin Forward: CCC ACC GTG TTC TTC GAC ATT

Cyclophilin Reverse: GGA CCC GTA TGC TTT AGG ATG A

Gel-Based ABPP

Gel-based ABPP methods were performed as previously described [43,64,65,69]. Recombinant pure human proteins were purchased from Origene. Pure proteins (0.1 µg) were pre-treated with DMSO vehicle or covalently-acting small molecules for 30 min at room temperature in an incubation volume of 50 µL PBS, and were subsequently treated with JNS-1-27 (50 µM final concentration) for 1 h at room temperature. CuAAC was performed to append rhodamine-azide (1 µM final concentration) onto alkyne probe-labeled proteins. Samples were then diluted with 20 µL of 4 x reducing Laemmli SDS sample loading buffer (Alfa Aesar) and heated at 90 °C for 5 min. The samples were separated on precast 4-20% TGX gels (Bio-Rad Laboratories, Inc.). Prior to scanning by ChemiDoc MP (Bio-Rad Laboratories, Inc), gels were fixed in a solution of 10% acetic acid, 30% ethanol for 2 hrs. Inhibition of target labeling was assessed by densitometry using ImageJ.

Synthesis and characterization of the nimbolide-alkyne probe and PROTACS XH1 and XH2

See supporting information for experimental details.

Synthesis and characterization of JNS27

See supporting information for experimental details.

Covalent Ligand Library

The synthesis and characterization of most of the covalent ligands screened against RNF114 have been previously reported [40,41,43,65]. Synthesis of TRH 1-156, TRH 1-160, TRH 1-167, YP 1-16, YP 1-22, YP 1-26, YP 1-31, YP 1-44 have been previously reported [70–77]. Compounds starting with "EN" were purchased from Enamine LLC. The synthesis and characterization of other covalent ligands not previously reported are described in **Supporting Information.**

Western blotting

Antibodies to RNF114 (Millipore Sigma, HPA021184), p21 (Cell Signaling Technology, 12D1), GAPDH (Proteintech Group Inc., 60004-1-Ig), BRD4 (Abcam plc, Ab128874), DYKDDDDK Tag (Cell Signaling Technology, D6W5B) and beta-actin (Proteintech Group Inc., 6609-1-Ig) were obtained from various commercial sources and dilutions were prepared per recommended manufacturers' procedures. Proteins were resolved by SDS/PAGE and transferred to nitrocellulose membranes using the iBlot system (Invitrogen). Blots were blocked with 5 % BSA in Tris-buffered saline containing Tween 20 (TBST) solution for 1 h at room temperature, washed in TBST, and probed with primary antibody diluted in recommended diluent per manufacturer overnight at 4 °C. Following washes with TBST, the blots were incubated in the dark with secondary antibodies purchased from Ly-Cor and used at 1:10,000 dilution in 5 % BSA in TBST at room temperature. Blots were visualized using an Odyssey Li-Cor scanner after additional washes. If additional primary antibody incubations were required the membrane was stripped using ReBlot Plus Strong Antibody Stripping Solution (EMD Millipore, 2504), washed and blocked again before being reincubated with primary antibody.

Expression and purification of wild-type and C8A RNF114

RNF114 was expressed and purified using several methods. In each case, RNF114 activity and sensitivity to nimbolide was confirmed. For the first method, we purchased wild-type mammalian expression plasmids with C-terminal FLAG tag were purchased from Origene (Origene Technologies Inc., RC209752). The RNF114 C8A mutant was generated with Q5 site-directed mutagenesis kit according to manufacturer's instructions (New England Biolabs, E0554S). Expression and purification conditions were optimized as reported previously [78]. HEK293T cells were grown to 60% confluency in DMEM (Corning) supplemented with 10 % FBS (Corning) and 2 mM L-glutamine (Life Technologies) and maintained at 37 °C with 5% CO_2. Immediately prior to transfection, media was replaced with DMEM containing 5 % FBS. Each plate was transfected with 20 µg of overexpression plasmid with 100 µg PEI (Sigma). After 48 h cells were collected in TBS, lysed by sonication, and batch bound with anti-DYKDDDDK resin (GenScript, L00432) for 90 min. Lysate and resin was loaded onto a gravity flow column and washed, followed by elution with 250 ng/µL 3 x FLAG peptide (ApexBio, A6001). Purity and concentration were verified by PAGE, UV/Spectroscopy, and BCA assay.

LC-MS/MS analysis of RNF114

Purified RNF114 (10 µg) in 50 µL PBS were incubated 30 min at room temperature either with DMSO vehicle or covalently acting compound (100 µM). The DMSO control was then treated with light IA while the compound treated sample was incubated with heavy IA for 1 h each at room temperature (200 µM final concentration, Sigma-Aldrich, 721328). The samples were precipitated by additional of 12.5 µL of 100% (w/v) TCA and the treated and control groups were combined pairwise, before cooling to -80 °C for 1 h. The combined sample was then spun for at max speed for 10 min at 4 °C, supernatant is carefully removed and the sample is washed with ice cold 0.01 M HCl/90 % acetone solution. The pellet was resuspended in 4 M urea containing 0.1 % Protease Max (Promega Corp. V2071) and diluted in 40 mM ammonium bicarbonate buffer. The samples were reduced with 10 mM TCEP at 60 °C for 30 min. The sample was then diluted 50% with PBS before sequencing grade trypsin (1 µg per sample, Promega Corp, V5111) was added for an overnight incubation at 37 °C. The next day the sample was centrifuged at 13200 rpm for 30 min. The supernatant was

transferred to a new tube and acidified to a final concentration of 5 % formic acid and stored at -80 °C until MS analysis.

RNF114 ubiquitination assay

Recombinant Myc-Flag-RNF114 proteins were either purified from HEK292T cells as described above or purchased from Origene (Origene Technologies Inc., TP309752). For *in vitro* auto-ubiquitination assay, 0.2 µg of RNF114 in 25 µL of TBS was pre-incubated with DMSO vehicle or the covalently-acting compound for 30 min at room temperature. Subsequently, 0.1 µg of UBE1 (Boston Biochem. Inc, E-305), 0.1 µg UBE2D1 (Boston Bichem. Inc, e2-615), 5 µg of Flag-ubiquitin (Boston Bichem. Inc, u-120) in a total volume of 25 µL Tris buffer containing 2 mM ATP, 10 mM DTT, and 10 mM $MgCl_2$ were added to achieve a final volume of 50 µL. The mixture was incubated at 37 °C with agitation for 1.5 h. 20 µL of Laemmli's buffer was added to quench the reaction and proteins were analyzed by western blot assay.

RNF114/p21 pulldown

Recombinant Flag-tagged RNF114 was used as bait to precipitate pure recombinant p21 (Origene Technologies Inc., TP309752 and TP720567) using Anti-Flag agarose beads (GenScript Biotech Corp., L00432). One microgram of Flag-RNF114 was added to 50 µL of TBS, followed by the addition of nimbolide (100 µM final concentration, Cayman Chemical Co., 19230) or equivalent volume of DMSO. Samples were incubated at room temperature for 30 min. One microgram of pure p21 was added to each sample, and samples were incubated at room temperature 30 min with agitation. Ten microliters of Flag agarose beads were added to each sample, and samples were agitated at room temperature for 30 min. Washes (3 times, 1 mL TBS) were performed before proteins were eluted using 50 µL of TBS supplemented with 250 ng/µL 3 x FLAG peptide (ApexBio A6001). Supernatant (30 µL) were collected and after the addition of Laemmli's reducing agent (10 µL), samples were boiled at 95 °C for 5 min and allowed to cool. Samples were analyzed by Western blotting as described above.

TMT-based quantitative proteomic profiling.

Cell Lysis, Proteolysis and Isobaric Labeling. Treated cell-pellets were lysed and digested using the commercially available Pierce™ Mass Spec Sample Prep Kit for Cultured Cells (Thermo Fisher Scientific, P/N 84840) following manufacturer's instructions. Briefly, 100 µg protein from each sample was reduced, alkylated, and digested overnight using a combination of Endoproteinase Lys-C and trypsin proteases. Individual samples were then labeled with isobaric tags using commercially available Tandem Mass Tag™ 6-plex (TMTsixplex™) (Thermo Fisher Scientific, P/N 90061) or TMT11plex (TMT11plex™) isobaric labeling reagent (Thermo Fisher Scientific, P/N 23275) kits, in accordance with manufacturer's protocols.

High pH Reversed Phase Separation. Tandem mass tag labeled (TMT) samples were then consolidated, and separated using high-pH reversed phase chromatography (RP-10) with fraction collection as previously described [79]. Fractions were speed-vac dried, then reconstituted to produce 24 fractions for subsequent on-line nanoLC-MS/MS analysis.

Protein Identification and Quantitation by nanoLC-MS/MS. Reconstituted RP-10 fractions were analyzed on a Thermo Orbitrap Fusion Lumos Mass Spectrometer (Xcalibur 4.1, Tune Application 3.0.2041) coupled to an EasyLC 1200 HPLC system (Thermo Fisher Scientific). The EasyLC 1200 was equipped with a 20 µL loop, set-up for 96 well plates. A Kasil-fritted trapping column (75 µm ID) packed with ReproSil-Pur 120 C18-AQ, 5 µm material (15mm bed length) was utilized together with a 160mm length, 75 µm inner diameter spraying capillary pulled to a tip diameter of approximately 8-10 µm using a P-2000 capillary puller (Sutter Instruments, Novato, CA). The 160mm separation column was packed with ReproSil-Pur 120 C18-AQ, 3 µm material (Dr. Maisch GmbH, Ammerbuch-Entringen, Germany). Mobile phase consisted of A= 0.1% formic acid/2% acetonitrile (v/v), and Mobile phase B= 0.1% formic acid/98% acetonitrile (v/v). Samples (18 µL) were injected on to trapping column using Mobile Phase A at a flow rate of 2.5 µL/min. Peptides were then eluted using an 80 minute gradient (2% Mobile Phase B for 5 min, 2%-40% B from 5-65 min, followed by 70% B from 65-70 minutes, then returning to 2% B from 70-80 min) at a flowrate of 300 nL/min on the capillary separation column with direct spraying into the mass spectrometer. Data was acquired on Orbitrap Fusion Lumos Mass Spectrometer in data-dependent mode using synchronous precursor scanning MS^3 mode (SPS-MS3), with MS^2 triggered for the 12 most intense precursor ions within a mass-to-charge ratio *(m/z)* range of 300-1500 found in the full MS survey scan event. MS scans were acquired at 60,000 mass resolution (*R*) at *m/z* 400, using a target value of 4×10^5 ions, and a maximum fill time of 50 ms. MS^2 scans were acquired as CID ion trap (IT) rapid type scans using a target value

of 1 x 10^4 ions, maximum fill time of 50 ms, and an isolation window of 2 Da. Data-dependent MS^3 spectra were acquired as Orbitrap (OT) scans, using Top 10 MS^2 daughter selection, automatic gain control (AGC) target of 5 x 10^4 ions, with scan range of *m/z* 100-500. The MS^3 maximum injection time was 86 ms, with HCD collision energy set to 65%. MS^3 mass resolution (*R*) was set to 15,000 at *m/z* 400 for TMT6plex experiments, and 50,000 at *m/z* 400 for TMT11-plex experiments. Dynamic exclusion was set to exclude selected precursors for 60 s with a repeat count of 1. Nanospray voltage was set to 2.2 kV, with heated capillary temperature set to 300 ºC, and an S-lens RF level equal to 30%. No sheath or auxiliary gas flow is applied.

Data Processing and Analysis. Acquired MS data was processed using Proteome Discoverer v. 2.2.0.388 software (Thermo) utilizing Mascot v 2.5.1 search engine (Matrix Science, London, UK) together with Percolator validation node for peptide-spectral match filtering [80]. Data was searched against Uniprot protein database (canonical human and mouse sequences, EBI, Cambridge, UK) supplemented with sequences of common contaminants. Peptide search tolearances were set to 10 ppm for precursors, and 0.8 Da for fragments. Trypsin cleavage specificity (cleavage at K, R except if followed by P) allowed for up to 2 missed cleavages. Carbamidomethylation of cysteine was set as a fixed modification, methionine oxidation, and TMT-modification of N-termini and lysine residues were set as variable modifications. Data validation of peptide and protein identifications was done at the level of the complete dataset consisting of combined Mascot search results for all individual samples per experiment via the Percolator validation node in Proteome Discoverer. Reporter ion ratio calculations were performed using summed abundances with most confident centroid selected from 20 ppm window. Only peptide-to-spectrum matches that are unique assignments to a given identified protein within the total dataset are considered for protein quantitation. High confidence protein identifications were reported using a Percolator estimated <1% false discovery rate (FDR) cut-off. Differential abundance significance was estimated using a backround-based ANOVA with Benjamini-Hochberg correction to determine adjusted p-values.

Tumor xenograft studies

Human tumor xenografts were established by transplanting cancer cells ectopically into the flank of female C.B17 severe combined immunodeficiency (SCID) mice (Taconic Farms) as previously described [68,81]. In brief, cells were washed with PBS, trypsinized, and harvested in serum-containing medium. Harvested cells were

washed in serum-free media and resuspended in serum-free media at a concentration of 2.0×10^4 cells/µl, and 100 µl was injected subcutaneously into the flank of each mouse. Tumors were measured with calipers. Animal experiments were conducted in accordance with the guidelines of the Institutional Animal Care and Use Committees of the University of California, Berkeley.

Data Availability Statement

The datasets generated during and/or analyzed during the current study are available from the corresponding author on reasonable request.

Acknowledgement

We thank the members of the Nomura Research Group, the Maimone lab, and Novartis Institutes for BioMedical Research for critical reading of the manuscript. We acknowledge Malte Moeller and Angus Olding for assistance in nimbolide isolation studies. We also acknowledge Andrew Proudfoot, Elizabeth Ornelas, Mikias Woldegiorgis from the Novartis Institutes for BioMedical Research for their assistance with protein expression and purification. This work was supported by Novartis Institutes for BioMedical Research and the Novartis-Berkeley Center for Proteomics and Chemistry Technologies (NB-CPACT) for all listed authors. This work was also supported by grants from the National Institutes of Health (R01CA172667 for DKN, JNS, CCW, LO; F31CA225173 for CCW).

References

1. Laraia, L., Robke, L. & Waldmann, H. Bioactive Compound Collections: From Design to Target Identification. *Chem* **4,** 705–730 (2018).
2. Koehn, F. E. & Carter, G. T. The evolving role of natural products in drug discovery. *Nat. Rev. Drug Discov.* **4,** 206–220 (2005).
3. Kingston, D. G. I. Modern Natural Products Drug Discovery and its Relevance to Biodiversity Conservation. *J. Nat. Prod.* **74,** 496–511 (2011).
4. Harvey, A. L., Edrada-Ebel, R. & Quinn, R. J. The re-emergence of natural products for drug discovery in the genomics era. *Nat. Rev. Drug Discov.* **14,** 111–129 (2015).

5. Nomura, D. K. & Maimone, T. J. Target Identification of Bioactive Covalently Acting Natural Products. *Curr. Top. Microbiol. Immunol.* (2018). doi:10.1007/82_2018_121

6. Wright, M. H. & Sieber, S. A. Chemical proteomics approaches for identifying the cellular targets of natural products. *Nat. Prod. Rep.* **33,** 681–708 (2016).

7. Drahl, C., Cravatt, B. F. & Sorensen, E. J. Protein-reactive natural products. *Angew. Chem. Int. Ed Engl.* **44,** 5788–5809 (2005).

8. Liu, J. *et al.* Calcineurin is a common target of cyclophilin-cyclosporin A and FKBP-FK506 complexes. *Cell* **66,** 807–815 (1991).

9. Cohen, E., Quistad, G. B. & Casida, J. E. Cytotoxicity of nimbolide, epoxyazadiradione and other limonoids from neem insecticide. *Life Sci.* **58,** 1075–1081 (1996).

10. Bodduluru, L. N., Kasala, E. R., Thota, N., Barua, C. C. & Sistla, R. Chemopreventive and therapeutic effects of nimbolide in cancer: the underlying mechanisms. *Toxicol. Vitro Int. J. Publ. Assoc. BIBRA* **28,** 1026–1035 (2014).

11. Subramani, R. *et al.* Nimbolide inhibits pancreatic cancer growth and metastasis through ROS-mediated apoptosis and inhibition of epithelial-to-mesenchymal transition. *Sci. Rep.* **6,** 19819 (2016).

12. Hao, F., Kumar, S., Yadav, N. & Chandra, D. Neem components as potential agents for cancer prevention and treatment. *Biochim. Biophys. Acta* **1846,** 247–257 (2014).

13. Chien, S.-Y. *et al.* Nimbolide induces apoptosis in human nasopharyngeal cancer cells. *Environ. Toxicol.* **32,** 2085–2092 (2017).

14. Elumalai, P. *et al.* Nimbolide inhibits invasion and migration, and down-regulates uPAR chemokine gene expression, in two breast cancer cell lines. *Cell Prolif.* **47,** 540–552 (2014).

15. Elumalai, P., Arunkumar, R., Benson, C. S., Sharmila, G. & Arunakaran, J. Nimbolide inhibits IGF-I-mediated PI3K/Akt and MAPK signalling in human breast cancer cell lines (MCF-7 and MDA-MB-231). *Cell Biochem. Funct.* **32,** 476–484 (2014).

16. Kavitha, K. *et al.* Nimbolide, a neem limonoid abrogates canonical NF-κB and Wnt signaling to induce caspase-dependent apoptosis in human hepatocarcinoma (HepG2) cells. *Eur. J. Pharmacol.* **681,** 6–14 (2012).

17. Pooladanda, V., Bandi, S., Mondi, S. R., Gottumukkala, K. M. & Godugu, C. Nimbolide epigenetically regulates autophagy and apoptosis in breast cancer. *Toxicol. Vitro Int. J. Publ. Assoc. BIBRA* **51,** 114–128 (2018).

18. Gupta, S. C. *et al.* Nimbolide, a limonoid triterpene, inhibits growth of human colorectal cancer xenografts by suppressing the proinflammatory microenvironment. *Clin. Cancer Res. Off. J. Am. Assoc. Cancer Res.* **19,** 4465–4476 (2013).

19. Lin, H., Qiu, S., Xie, L., Liu, C. & Sun, S. Nimbolide suppresses non-small cell lung cancer cell invasion and migration via manipulation of DUSP4 expression and ERK1/2 signaling. *Biomed. Pharmacother. Biomedecine Pharmacother.* **92,** 340–346 (2017).

20. Babykutty, S. *et al.* Nimbolide retards tumor cell migration, invasion, and angiogenesis by downregulating MMP-2/9 expression via inhibiting ERK1/2 and reducing DNA-binding activity of NF-κB in colon cancer cells. *Mol. Carcinog.* **51,** 475–490 (2012).

21. Nagini, S. Neem Limonoids as Anticancer Agents: Modulation of Cancer Hallmarks and Oncogenic Signaling. *The Enzymes* **36,** 131–147 (2014).

22. Alshammari, G. M., Balakrishnan, A. & Chinnasamy, T. Nimbolide attenuate the lipid accumulation, oxidative stress and antioxidant in primary hepatocytes. *Mol. Biol. Rep.* **44,** 463–474 (2017).

23. Leslie, B. J. & Hergenrother, P. J. Identification of the cellular targets of bioactive small organic molecules using affinity reagents. *Chem. Soc. Rev.* **37,** 1347–1360 (2008).

24. Pan, S., Zhang, H., Wang, C., Yao, S. C. L. & Yao, S. Q. Target identification of natural products and bioactive compounds using affinity-based probes. *Nat. Prod. Rep.* **33,** 612–620 (2016).

25. Ursu, A. & Waldmann, H. Hide and seek: Identification and confirmation of small molecule protein targets. *Bioorg. Med. Chem. Lett.* **25,** 3079–3086 (2015).

26. Burslem, G. M. & Crews, C. M. Small-Molecule Modulation of Protein Homeostasis. *Chem. Rev.* **117,** 11269–11301 (2017).

27. Zengerle, M., Chan, K.-H. & Ciulli, A. Selective Small Molecule Induced Degradation of the BET Bromodomain Protein BRD4. *ACS Chem. Biol.* **10,** 1770–1777 (2015).

28. Lai, A. C. & Crews, C. M. Induced protein degradation: an emerging drug discovery paradigm. *Nat. Rev. Drug Discov.* **16,** 101–114 (2017).

29. Neklesa, T. K., Winkler, J. D. & Crews, C. M. Targeted protein degradation by PROTACs. *Pharmacol. Ther.* (2017). doi:10.1016/j.pharmthera.2017.02.027

30. Winter, G. E. *et al.* DRUG DEVELOPMENT. Phthalimide conjugation as a strategy for in vivo target protein degradation. *Science* **348,** 1376–1381 (2015).

31. Shortt, J., Ott, C. J., Johnstone, R. W. & Bradner, J. E. A chemical probe toolbox for dissecting the cancer epigenome. *Nat. Rev. Cancer* **17,** 160–183 (2017).

32. Sakamoto, K. M. *et al.* Protacs: chimeric molecules that target proteins to the Skp1-Cullin-F box complex for ubiquitination and degradation. *Proc. Natl. Acad. Sci. U. S. A.* **98,** 8554–8559 (2001).

33. Schneekloth, J. S. *et al.* Chemical genetic control of protein levels: selective in vivo targeted degradation. *J. Am. Chem. Soc.* **126,** 3748–3754 (2004).

34. Lu, J. *et al.* Hijacking the E3 Ubiquitin Ligase Cereblon to Efficiently Target BRD4. *Chem. Biol.* **22,** 755–763 (2015).

35. Bianchini, G., Balko, J. M., Mayer, I. A., Sanders, M. E. & Gianni, L. Triple-negative breast cancer: challenges and opportunities of a heterogeneous disease. *Nat. Rev. Clin. Oncol.* **13,** 674–690 (2016).

36. Zeichner, S. B., Terawaki, H. & Gogineni, K. A Review of Systemic Treatment in Metastatic Triple-Negative Breast Cancer. *Breast Cancer Basic Clin. Res.* **10,** 25–36 (2016).

37. Weerapana, E. *et al.* Quantitative reactivity profiling predicts functional cysteines in proteomes. *Nature* **468,** 790–795 (2010).

38. Evans, M. J. & Cravatt, B. F. Mechanism-based profiling of enzyme families. *Chem. Rev.* **106,** 3279–3301 (2006).

39. Roberts, A. M., Ward, C. C. & Nomura, D. K. Activity-based protein profiling for mapping and pharmacologically interrogating proteome-wide ligandable hotspots. *Curr. Opin. Biotechnol.* **43,** 25–33 (2017).

40. Grossman, E. A. *et al.* Covalent Ligand Discovery against Druggable Hotspots Targeted by Anti-cancer Natural Products. *Cell Chem. Biol.* **24,** 1368-1376.e4 (2017).

41. Roberts, A. M. *et al.* Chemoproteomic Screening of Covalent Ligands Reveals UBA5 As a Novel Pancreatic Cancer Target. *ACS Chem. Biol.* **12,** 899–904 (2017).

42. Anderson, K. E., To, M., Olzmann, J. A. & Nomura, D. K. Chemoproteomics-Enabled Covalent Ligand Screening Reveals a Thioredoxin-Caspase 3 Interaction Disruptor That Impairs Breast Cancer Pathogenicity. *ACS Chem. Biol.* **12,** 2522–2528 (2017).

43. Counihan, J. L., Wiggenhorn, A. L., Anderson, K. E. & Nomura, D. K. Chemoproteomics-Enabled Covalent Ligand Screening Reveals ALDH3A1 as a Lung Cancer Therapy Target. *ACS Chem. Biol.* (2018). doi:10.1021/acschembio.8b00381

44. Backus, K. M. *et al.* Proteome-wide covalent ligand discovery in native biological systems. *Nature* **534,** 570–574 (2016).

45. Wang, C., Weerapana, E., Blewett, M. M. & Cravatt, B. F. A chemoproteomic platform to quantitatively map targets of lipid-derived electrophiles. *Nat. Methods* **11,** 79–85 (2014).

46. Hacker, S. M. *et al.* Global profiling of lysine reactivity and ligandability in the human proteome. *Nat. Chem.* **advance online publication,** (2017).

47. Ward, C. C., Kleinman, J. I. & Nomura, D. K. NHS-Esters As Versatile Reactivity-Based Probes for Mapping Proteome-Wide Ligandable Hotspots. *ACS Chem. Biol.* **12,** 1478–1483 (2017).

48. Han, J. *et al.* ZNF313 is a novel cell cycle activator with an E3 ligase activity inhibiting cellular senescence by destabilizing p21(WAF1.). *Cell Death Differ.* **20,** 1055–1067 (2013).

49. Ma, Y.-X. *et al.* Identification of a novel human zinc finger protein gene ZNF313. *Sheng Wu Hua Xue Yu Sheng Wu Wu Li Xue Bao Acta Biochim. Biophys. Sin.* **35,** 230–237 (2003).

50. Lee, M.-G. *et al.* XAF1 directs apoptotic switch of p53 signaling through activation of HIPK2 and ZNF313. *Proc. Natl. Acad. Sci. U. S. A.* **111,** 15532–15537 (2014).

51. Huang, S. *et al.* The UbL-UBA Ubiquilin4 protein functions as a tumor suppressor in gastric cancer by p53-dependent and p53-independent regulation of p21. *Cell Death Differ.* (2018). doi:10.1038/s41418-018-0141-4

52. Havens, C. G. & Walter, J. C. Mechanism of CRL4(Cdt2), a PCNA-dependent E3 ubiquitin ligase. *Genes Dev.* **25,** 1568–1582 (2011).

53. Kitagawa, K., Kotake, Y. & Kitagawa, M. Ubiquitin-mediated control of oncogene and tumor suppressor gene products. *Cancer Sci.* **100,** 1374–1381 (2009).

54. Biswas, K. *et al.* The E3 Ligase CHIP Mediates p21 Degradation to Maintain Radioresistance. *Mol. Cancer Res. MCR* **15,** 651–659 (2017).

55. Rodriguez, M. S. *et al.* The RING ubiquitin E3 RNF114 interacts with A20 and modulates NF-κB activity and T-cell activation. *Cell Death Dis.* **5,** e1399 (2014).

56. Yang, Y. *et al.* The E3 ubiquitin ligase RNF114 and TAB1 degradation are required for maternal-to-zygotic transition. *EMBO Rep.* **18,** 205–216 (2017).

57. Rape, M. Ubiquitylation at the crossroads of development and disease. *Nat. Rev. Mol. Cell Biol.* **19,** 59–70 (2018).

58. Hughes, S. J. & Ciulli, A. Molecular recognition of ternary complexes: a new dimension in the structure-guided design of chemical degraders. *Essays Biochem.* **61,** 505–516 (2017).

59. Chamberlain, P. P. *et al.* Structure of the human Cereblon-DDB1-lenalidomide complex reveals basis for responsiveness to thalidomide analogs. *Nat. Struct. Mol. Biol.* **21,** 803–809 (2014).

60. Krönke, J. *et al.* Lenalidomide induces ubiquitination and degradation of CK1α in del(5q) MDS. *Nature* **523,** 183–188 (2015).

61. Gadd, M. S. *et al.* Structural basis of PROTAC cooperative recognition for selective protein degradation. *Nat. Chem. Biol.* **13,** 514–521 (2017).

62. Nowak, R. P. *et al.* Plasticity in binding confers selectivity in ligand-induced protein degradation. *Nat. Chem. Biol.* (2018). doi:10.1038/s41589-018-0055-y

63. Jessani, N. *et al.* Carcinoma and stromal enzyme activity profiles associated with breast tumor growth in vivo. *Proc. Natl. Acad. Sci. U. S. A.* **101,** 13756–13761 (2004).

64. Louie, S. M. *et al.* GSTP1 Is a Driver of Triple-Negative Breast Cancer Cell Metabolism and Pathogenicity. *Cell Chem. Biol.* **23,** 567–578 (2016).

65. Bateman, L. A. *et al.* Chemoproteomics-enabled covalent ligand screen reveals a cysteine hotspot in reticulon 4 that impairs ER morphology and cancer pathogenicity. *Chem. Commun. Camb. Engl.* **53,** 7234–7237 (2017).

66. Smith, P. K. *et al.* Measurement of protein using bicinchoninic acid. *Anal. Biochem.* **150,** 76–85 (1985).

67. Xu, T. *et al.* ProLuCID: An improved SEQUEST-like algorithm with enhanced sensitivity and specificity. *J. Proteomics* **129,** 16–24 (2015).

68. Benjamin, D. I. *et al.* Ether lipid generating enzyme AGPS alters the balance of structural and signaling lipids to fuel cancer pathogenicity. *Proc. Natl. Acad. Sci. U. S. A.* **110,** 14912–14917 (2013).

69. Medina-Cleghorn, D. *et al.* Mapping Proteome-Wide Targets of Environmental Chemicals Using Reactivity-Based Chemoproteomic Platforms. *Chem. Biol.* **22,** 1394–1405 (2015).

70. Kokosza, K., Balzarini, J. & Piotrowska, D. G. Novel 5-Arylcarbamoyl-2-methylisoxazolidin-3-yl-3-phosphonates as Nucleotide Analogues. *Nucleosides Nucleotides Nucleic Acids* **33,** 552–582 (2014).

71. Talaty, E. R., Young, S. M., Dain, R. P. & Stipdonk, M. J. V. A study of fragmentation of protonated amides of some acylated amino acids by tandem mass spectrometry: observation of an unusual nitrilium ion. *Rapid Commun. Mass Spectrom.* **25,** 1119–1129 (2011).

72. Timokhin, V. I., Gastaldi, S., Bertrand, M. P. & Chatgilialoglu, C. Rate Constants for the β-Elimination of Tosyl Radical from a Variety of Substituted Carbon-Centered Radicals. *J. Org. Chem.* **68,** 3532–3537 (2003).

73. Cee, V. J. *et al.* Systematic Study of the Glutathione (GSH) Reactivity of N-Arylacrylamides: 1. Effects of Aryl Substitution. *J. Med. Chem.* **58,** 9171–9178 (2015).

74. Le Sann, C., Huddleston, J. & Mann, J. Synthesis and preliminary evaluation of novel analogues of quindolines as potential stabilisers of telomeric G-quadruplex DNA. *Tetrahedron* **63,** 12903–12911 (2007).

75. Ikoma, M., Oikawa, M. & Sasaki, M. Synthesis and domino metathesis of functionalized 7-oxanorbornene analogs toward cis-fused heterocycles. *Tetrahedron* **64,** 2740–2749 (2008).

76. Cho, S.-D. *et al.* A One-Pot Synthesis of Pyrido[2,3-b][1,4]oxazin-2-ones. *J. Org. Chem.* **68,** 7918–7920 (2003).

77. Magolan, J., Carson, C. A. & Kerr, M. A. Total Synthesis of (±)-Mersicarpine. *Org. Lett.* **10,** 1437–1440 (2008).

78. Longo, P. A., Kavran, J. M., Kim, M.-S. & Leahy, D. J. Transient mammalian cell transfection with polyethylenimine (PEI). *Methods Enzymol.* **529,** 227–240 (2013).

79. Thomas, J. R. *et al.* A Photoaffinity Labeling-Based Chemoproteomics Strategy for Unbiased Target Deconvolution of Small Molecule Drug Candidates. *Methods Mol. Biol. Clifton NJ* **1647,** 1–18 (2017).

80. Käll, L., Canterbury, J. D., Weston, J., Noble, W. S. & MacCoss, M. J. Semi-supervised learning for peptide identification from shotgun proteomics datasets. *Nat. Methods* **4,** 923–925 (2007).

81. Nomura, D. K. *et al.* Monoacylglycerol lipase regulates a fatty acid network that promotes cancer pathogenesis. *Cell* **140,** 49–61 (2010).

Figure Legends

Figure 1. Nimbolide impairs breast cancer cell proliferation or survival. (A) Structure of nimbolide. Nimbolide possesses a cyclic enone that is potentially cysteine-reactive. **(B)** 231MFP and HCC38 breast cancer cell proliferation in serum-containing media and serum-free cell survival. Cells were treated with DMSO vehicle or nimbolide and cell viability was assessed after 48 h by Hoechst stain. Data shown in **(B)** are average ± sem, n=6/group. Significance is expressed as *p<0.05 compared to vehicle-treated controls.

Figure 2. isoTOP-ABPP analysis of nimbolide in 231MFP breast cancer cell proteomes reveal RNF114 as a target. (A) Schematic of isoTOP-ABPP in which breast cancer cell proteomes or cells were pre-treated with DMSO or nimbolide (10 μM, 1.5 h *in situ*) prior to labeling of proteomes *in vitro* with IA-alkyne (100 μM, 1 h), followed by appendage of isotopically light (for DMSO-treated) or heavy (for nimbolide-treated) TEV protease cleavable biotin-azide tags by copper-catalyzed azide-alkyne cycloaddition (CuAAC). Control and treated proteomes were subsequently combined in a 1:1 ratio, probe-labeled proteins were avidin-enriched, digested with trypsin, and probe-modified tryptic peptides were eluted by TEV protease, analyzed by LC-MS/MS, and light to heavy probe-modified peptide ratios were quantified. **(B)** isoTOP-ABPP analysis of nimbolide (10 μM) in 231MFP breast cancer cells *in situ* analyzed as described in **(A). (C)** RNF114 was stably knocked down using a short-hairpin RNA oligonucleotide in 231MFP cells. RNF114 knockdown in shRNF114 cells was confirmed by qPCR in comparison to shControl cells. Cell proliferation was assessed 48 h after seeding cells by Hoechst stain. **(D)** 231MFP shControl and shRNF114 sensitivity to nimbolide. 231MFP shControl and shRNF114 cells were treated with DMSO vehicle or nimbolide and cell proliferation was assessed after 48 h by Hoechst stain. % proliferation with nimbolide treatment was normalized against respective shControl or shRNF114 control groups. Data shown in **(C-D)** are average ± sem. Data shown in **(B-D)** are from n=6/group. Significance in **(C, D)** is expressed as *p<0.05 compared to shControl groups.

Figure 3. Nimbolide reacts covalently with C8 of RNF114. (A) Nimbolide targets an intrinsically disordered region within RNF114 as assessed by PONDR. **(B)** Route for synthesis of the alkyne-functionalized nimbolide probe. **(C)** Gel-based ABPP analysis of pure human RNF114 protein labeled with nimbolide probe. In the

upper two panels, pure RNF114 protein was pre-incubated with DMSO vehicle or nimbolide (100 μM, 30 min) prior to labeling with the nimbolide probe (10 μM, 1 h) in PBS. In the lower two panels, pure wild-type and C8A mutant RNF114 protein were labeled with the nimbolide probe (10 μM, 1 h) in PBS with 1 mg/ml BSA. For both experiments, shown are nimbolide-alkyne labeling and silver staining of RNF114. **(D)** Pure RNF114 protein was labeled with nimbolide (100 μM, 1 h) and subjected to tryptic digestion and LC-MS/MS analysis. Shown is the nimbolide-modified adduct on C8 of RNF114. Data shown in **(C)** are from n=3/group.

Figure 4. Nimbolide inhibits RNF114 activity through disrupting substrate recognition. (A) RNF114 ubiquitination assay with pure GST-Ube1, GST-UBE2D1, and RNF114 protein, Flag-Ubiquitin and ATP with or without addition of p21 and blotting against Flag-ubiquitin (left) or p21 (right). DMSO or Nimbolide (100 μM) was pre-incubated with RNF114, before the addition of the E1 and E2 enzymes, Flag-ubiquitin and ATP to start the reaction. **(B)** RNF114 autoubiquitination assay with DMSO or nimbolide (100 μM) treatment with wild-type or C8A mutant RNF114. **C)** In an *in vitro* incubation of pure RNF114 and p21 protein, Flag-RNF114 pulldown and p21 enrichment was inhibited by nimbolide (100 μM). **D)** 231MFP cells were treated with nimbolide (100 μM). Shown are p21 levels in DMSO control or nimbolide-treated cells. Gels shown in **(A-D)** are representative images from n=3/group. Data shown in **(C)** are average ± sem. Data shown in **(C)** are from n=3/group. Significance in **(C)** is expressed as *p<0.05 compared to the p21/RNF114 group in **(C)** or against vehicle-treated control groups for each time point in **(D)**.

Figure 5. Nimbolide can be used to recruit RNF114 for targeted protein degradation of BRD4. (A) Route for synthesizing XH2, a nimbolide-based degrader consisting of nimbolide as an RNF114 recruiter, a linker, and the BRD4 inhibitor JQ1. **(B)** BRD4 levels in 231MFP breast cancer cells treated with MZ1 versus XH2 treatment for 12 h. **(C-D)** BRD4 levels in 231MFP breast cancer cells pre-treated with DMSO vehicle or proteasome inhibitor bortezomib (BTZ) (1 μM) **(C)** or E1 ubiquitin activating enzyme inhibitor TAK-243 (10 μM) **(D)** 30 min prior to and also during treatment with MZ1 (1 μM) or XH2 (100 nM) treatment (100 nM) for 12 h. **(E)** RNF114 and BRD4 expression in RNF114 wild-type (WT) or knockout (KO) HAP1 cells treated with DMSO vehicle, MZ1 (1 μM), or XH2 (100 nM) for 12 h. **(F, G)** Tandem mass tag (TMT)-based quantitative proteomic profiling of 231MFP breast cancer cells treated with DMSO vehicle or XH2 (100 nM) **(F)** or DMSO vehicle or

nimbolide (100 nM) for 12 h **(G)**. Long and short BRD4 isoforms in **(B-E)** were visualized by SDS/PAGE and Western blotting, quantified by densitometry, and normalized to GAPDH loading controls in **(B-E)**. Gels shown in **(B-E)** are representative images from n=3/group. Data shown in **(F** and **G)** are for 5797 and 6397 protein groups quantified with 2 or more unique peptides in triplicate treatments, see **Table S2** for details. Data shown in **(B-E)** are average ± sem. Significance in **(B-E)** is expressed as *p<0.05 compared to the vehicle-treated control groups and #p<0.05 compared to XH2-treated groups in **(B-D)** or to the WT XH2-treated group **(E)**.

Figure 6. Chemoproteomics-enabled covalent ligand screening to identify more synthetically tractable covalent ligands against RNF114. (A) Gel-based ABPP analysis of nimbolide competition against IA-alkyne (10 μM) or JNS27 (50 μM) labeling of pure RNF114 protein. Structures of IA-alkyne and JNS27 probes are shown with reactive moieties highlighted in red. Shown also is gel-based ABPP analysis of nimbolide (50 μM) competition against JNS27 labeling of wild-type and C8A mutant RNF114 protein. In these experiments, DMSO or nimbolide was pre-incubated for 30 min prior to probe labeling for 1 h. **(B)** Upon screening a library of cysteine-reactive covalent ligands against JNS27 labeling of RNF114, EN62 was one of the top hits. Shown is the structure of EN62 with the acrylamide reactive moiety highlighted in red. Shown also is a gel-based ABPP analysis of EN62 against JNS27 labeling of pure RNF114. **(C)** RNF114 autoubiquitination assay with DMSO or EN62 (50 μM) treatment with wild-type or C8A mutant RNF114. **(D)** IsoTOP-ABPP analysis of EN62 in 231MFP breast cancer cell proteomes *in vitro*. DMSO or EN62 (50 μM) were pre-incubated with 231MFP proteomes 30 min prior to IA-alkyne labeling (100 μM) for 1 h, followed by the isoTOP-ABPP method. **(E)** 231MFP cell survival with EN62 after 48 h assessed by Hoechst stain. **(F)** 231MFP tumor xenograft growth in C.B-17 female SCID mice treated with vehicle (18:1:1 saline:PEG40:ethanol) or EN62 (50 mg/kg ip, once per day, initiated 17 days after subcutaneous injection of 231MFP cells). Gels shown in **(A-C)** are representative images from n=3/group. Data shown in **(D, F)** are average ± sem, n=3-8/group. Significance in **(E,F)** is expressed as *p<0.05 compared to the vehicle-treated controls.

Figure 1

A

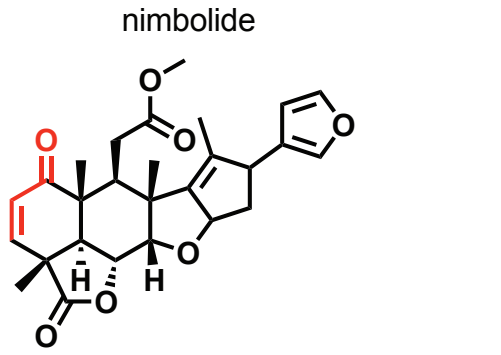

B

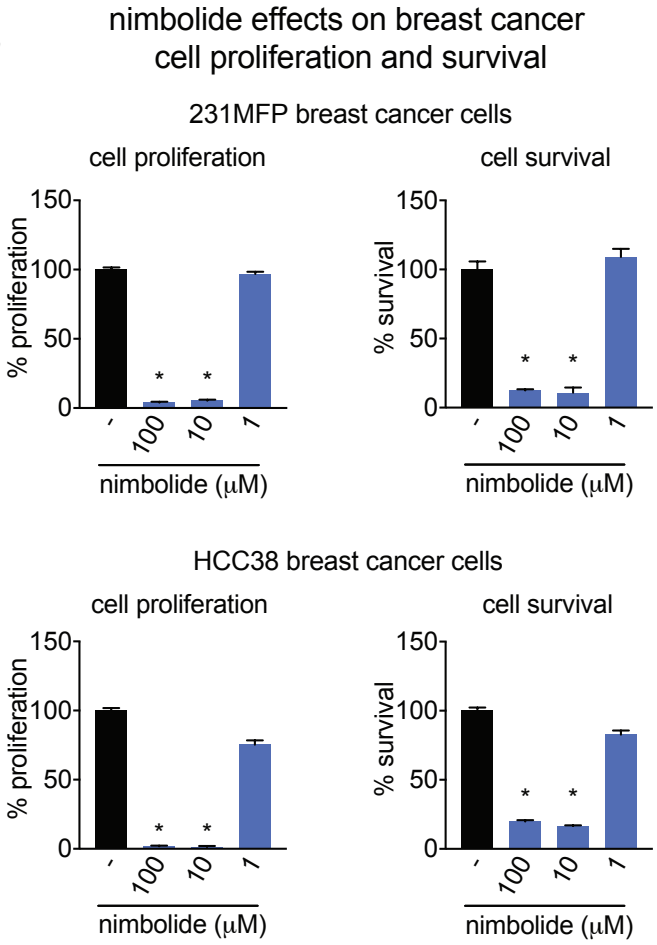

Figure 2

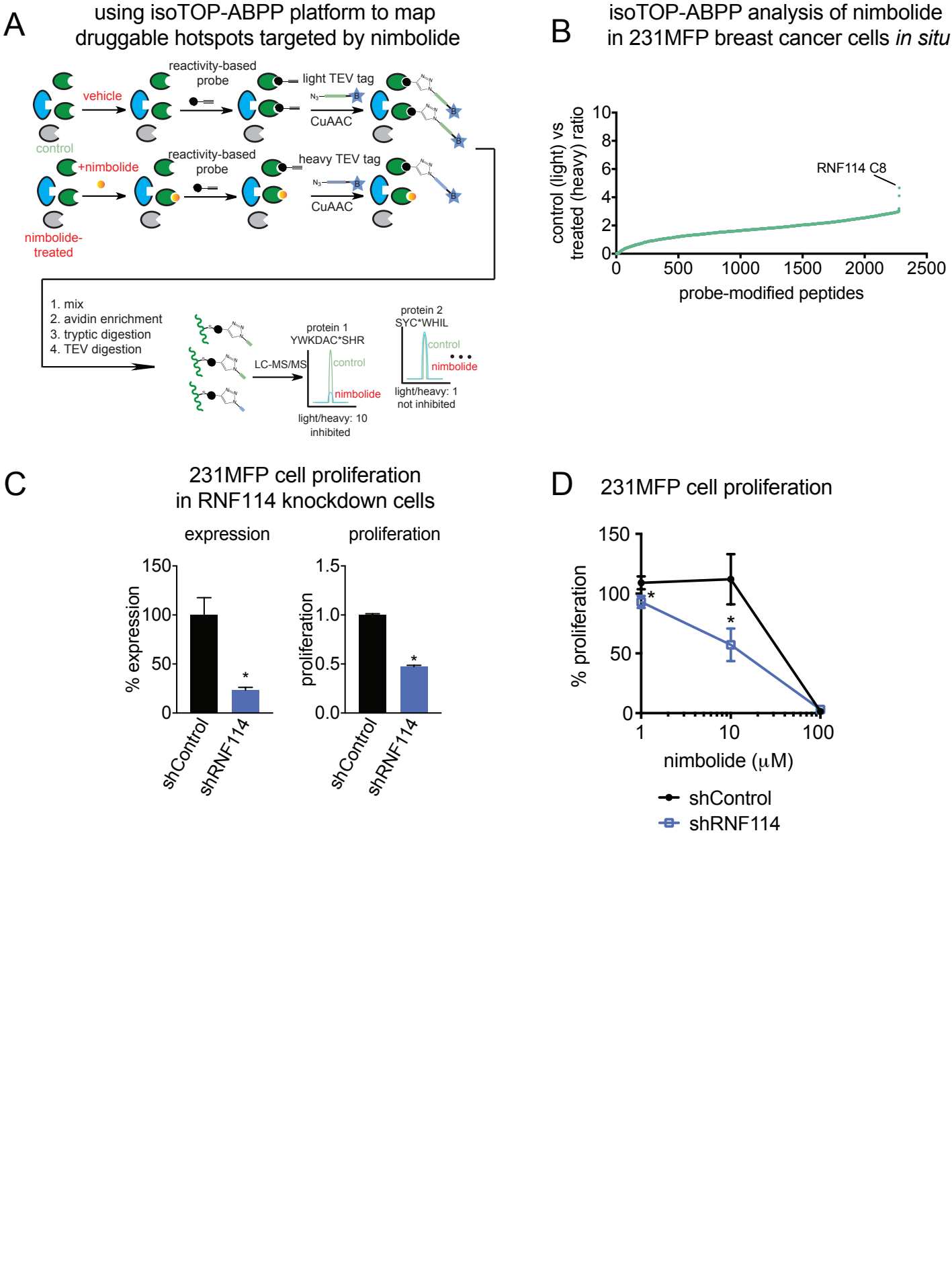

Figure 3

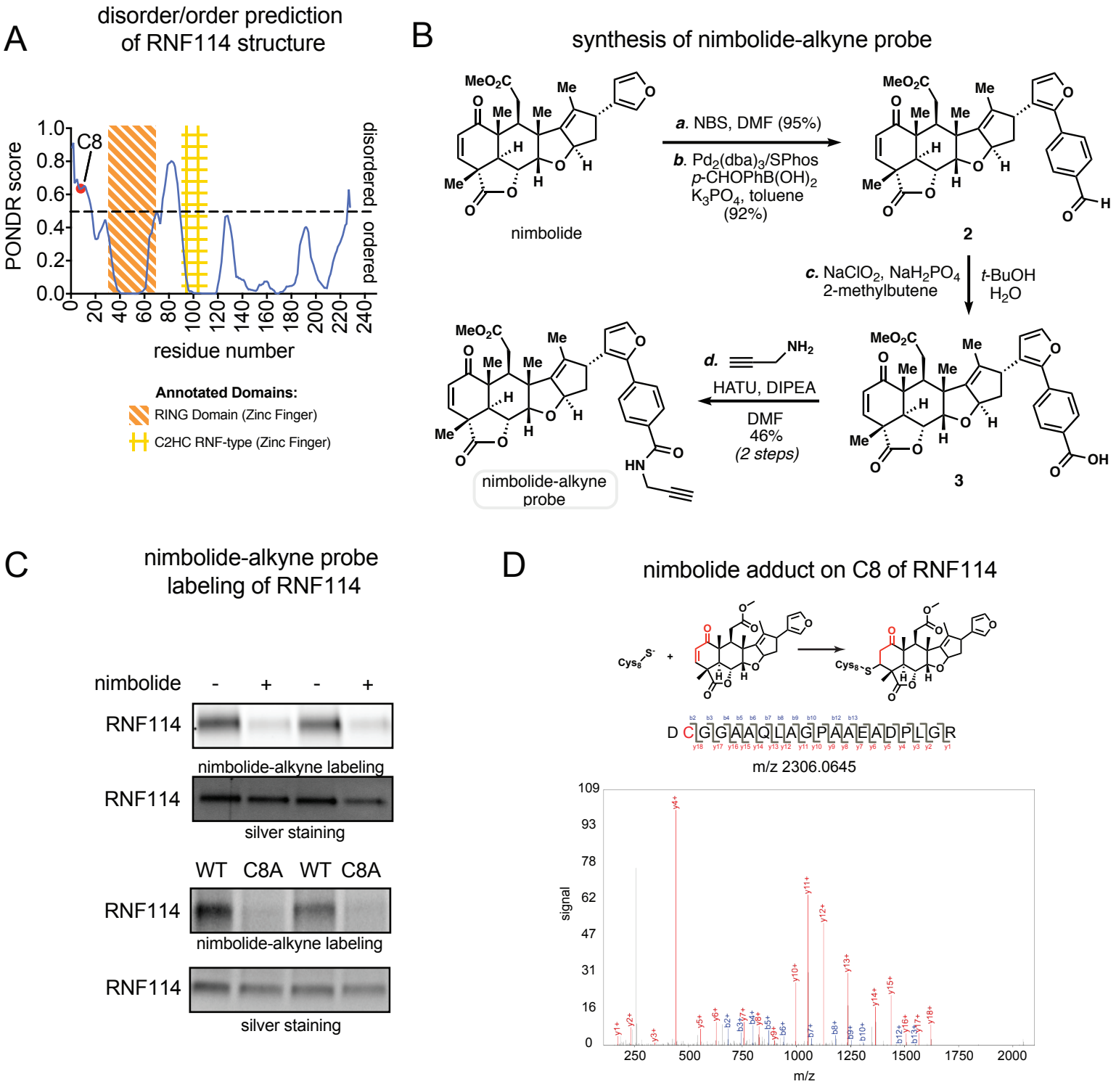

Figure 4

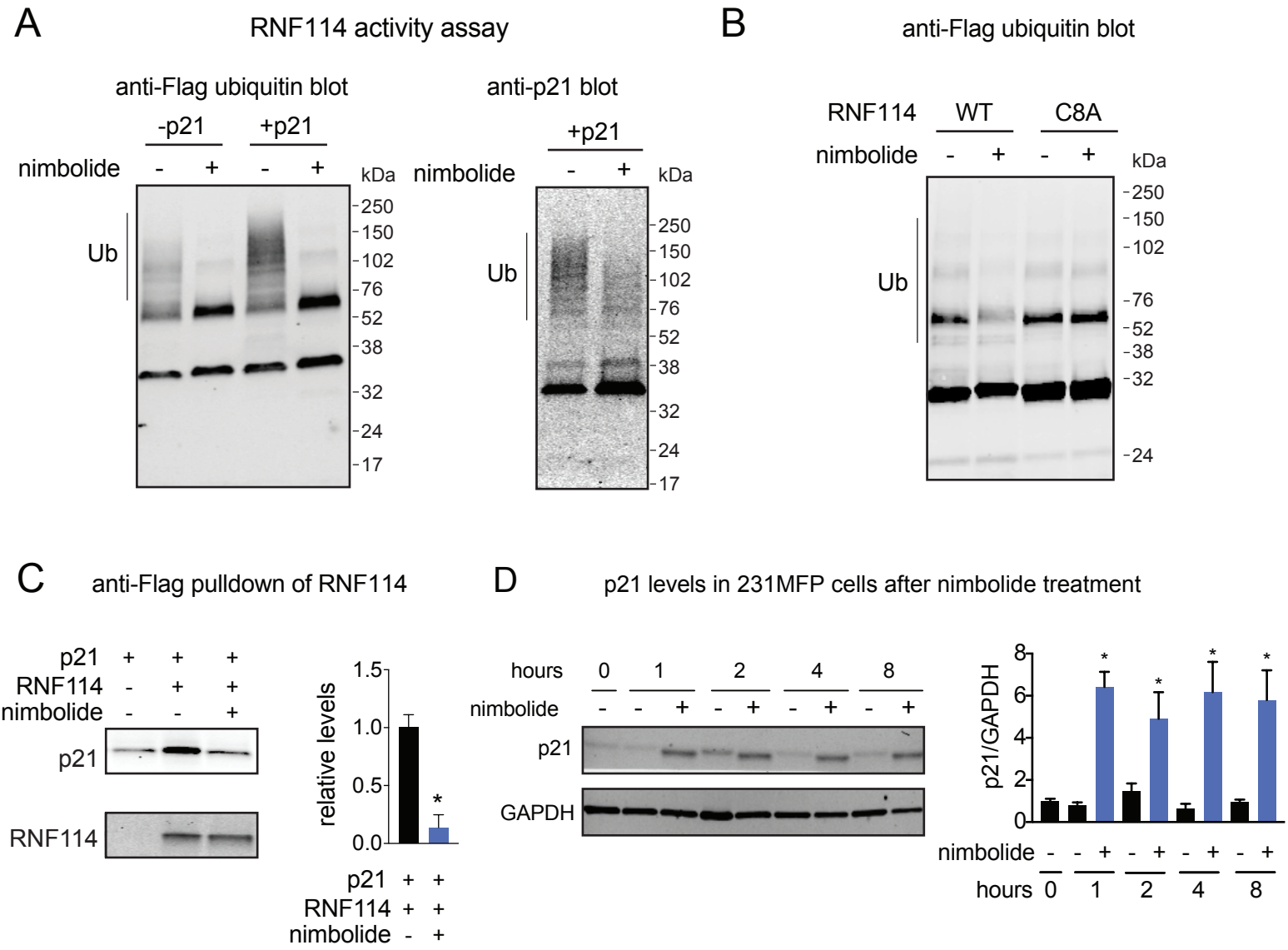

Figure 5

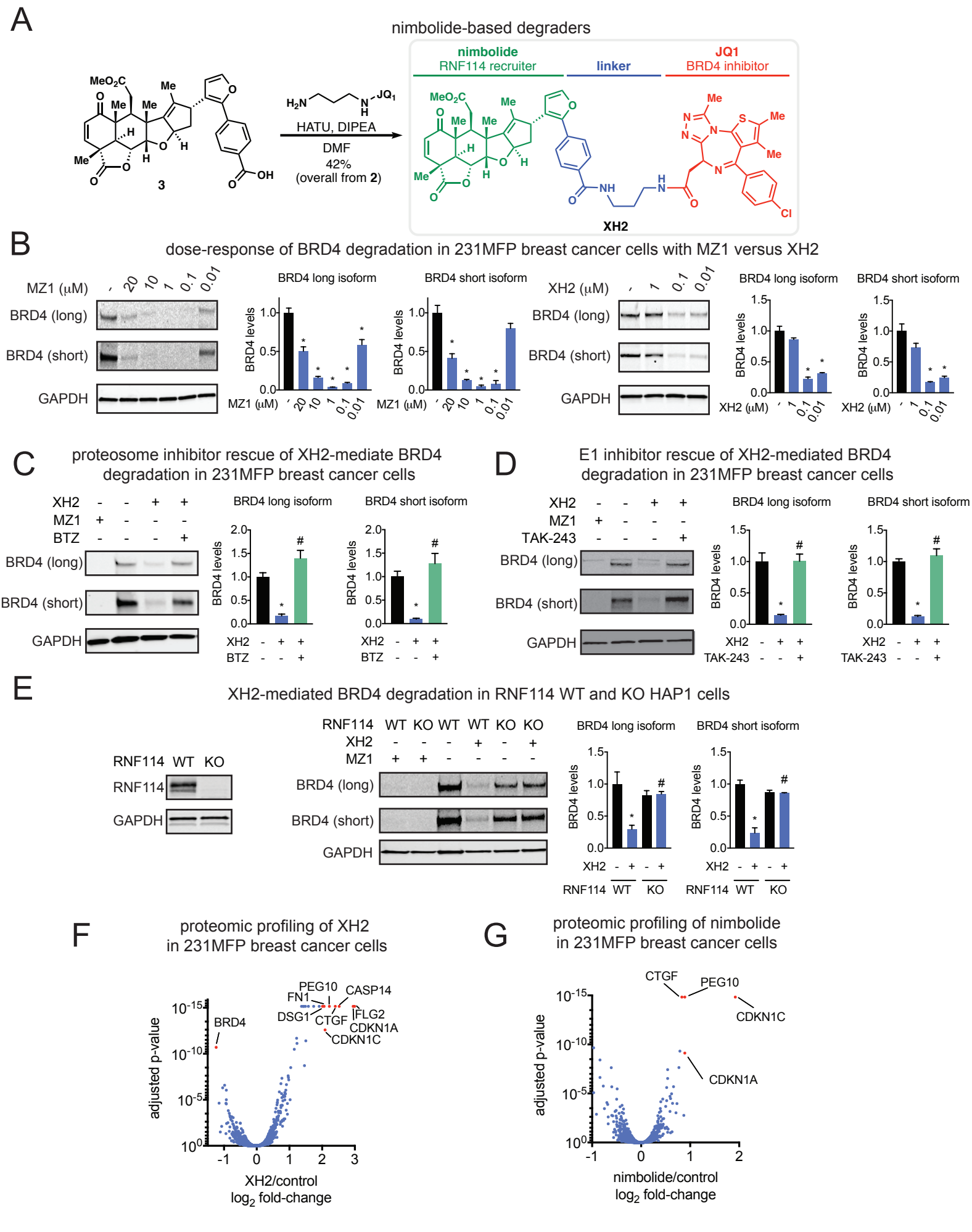

Figure 6